



Numerical Investigations on a Small-Scale Air-Slide Conveyor

J. Xiang^{1,2,†} and T. H. New¹

¹ Nanyang Technological University, School of Mechanical and Aerospace Engineering, Singapore 639798

² CSIRO Manufacturing, Private Bag 10, Normanby Road, Clayton, VIC 3168, Australia

†Corresponding Author Email: jerry.xiang@csiro.au

(Received May 22, 2018; accepted July 25, 2018)

ABSTRACT

This study reports upon numerical investigations on a small-scale air-slide conveyor (ASC) model that is based on a full-scale industrial ASC currently in operation. For validation of the ASC model and prediction of details of cement flow distribution on time-basis, both steady-state and transient simulations are performed. Simulation results demonstrate the development of cement flow phenomenon and predict critical flow features in the system, which will be useful for predicting corresponding behavior in the full-scale industrial ASC. Mass balance is achieved and potential optimization technique is supported by simulation data. Both steady-state converged solution and results on time-basis are discussed. This study demonstrates the validity of ASC model design and paves the way for using similar numerical tools for future particle-laden flow studies. Lastly, it also offers design and optimization insights into such industrial ASC systems.

Keywords: Air-slide conveyor; Cement flow; Numerical simulation; Prototype.

NOMENCLATURE

ASC	air-slide conveyor	U_0	fluid velocity of flow
d_p	particle diameter	VelMag	velocity magnitude
L_0	characteristic dimension of the actual model	\square	incline angle
\dot{m}	mass flow rate	ρ_p	particle density
$p_{suction}$	suction pressure	ρ_{bulk}	bulk density
S_i	Stokes number	μ	air dynamics viscosity
SLR	solid loading ratio		

1. INTRODUCTION

Pneumatic conveying systems based on air-slide conveyor or pneumatic pipes are efficient ways to transport powdery materials and used for a wide range of engineering applications (Cong *et al.* 2011; Setia and Mallick 2015a). The efficiency and effectiveness of pneumatic system impact on the delivery of powdery materials significantly and thus influence the entire logistic chain. To better understand and improve operations related components of pneumatic systems, both experimental and numerical techniques have been utilized to study them (Gupta *et al.* 2009; Li *et al.* 2014). Take for instance, Yan and Rinoshika (2013) conducted PIV measurement to determine particle concentration and velocity, revealing the mechanism of conveying velocity reduction and drops of pressure in a self-excited horizontal

pneumatic conveying through the use of soft fins. Particle Image Velocimetry (PIV) proved to be an efficient technique to reveal the details of particle distributions, as demonstrated in other studies as well (New and Tsioli 2011; New and Long 2015). Gupta *et al.* (2006) investigated dry particulate materials transportation at different conveyor inclinations when a fluidized system with a length of 3.7 meter is used. Increasing the superficial air velocity increases the mass flow rate of material and the mass flow rate of solids shows a decreasing trend when the orientation of conveyor was changed from downward to upward. Mittal *et al.* (2015) investigated the mechanism of flow, associating it with fluidized dense phase to dilute phase pneumatic conveying of fine powders. Three different analysis methods for signal were applied to the obtained pressure fluctuations, to reveal the nature of flow within the pipelines.

Li *et al.* (2014) investigated the influence of material properties numerically, to understand how the conveying is affected for horizontal pneumatic system, where CFD method is combined with the discrete element method (DEM). The particle solid concentration, velocity and drop of pressure were influenced by the particle restitution coefficients as well as friction. Pu *et al.* (2010) adjusted the kinetic-friction model to the two-fluid model, to investigate the pneumatic conveying of dense-phase pulverized coal. Simulation predicted pressure gradients as well as solid concentration distribution presented good agreement with experiments and electrical capacitance tomography image. Lungu *et al.* (2015) attempted to model flow structures and coefficients of heat transfer in a fluidized bed where a central jet is operated. The simulation results predicted that maximum instantaneous local fluid-to-particle coefficients occur in bubble wakes. Wang *et al.* (2016) pioneered by using Lattice Boltzmann Method (LBM) simulations to investigate particle-laden turbulent channel flows. The LBM results well agreed with results derived from finite-difference methods, thus demonstrated the potential accuracy and efficiency of LBM in treating particle-laden turbulent flows. Almohammed and Breuer (2016a) compared agglomeration models which are energy-based and momentum-based respectively in turbulent particle-laden flows through large-eddy simulations. The comparative study revealed possible reasons for slight deviations between simulation results from the two models. Wang *et al.* (2017) recently presented results from direct numerical simulations where a particle-laden plane turbulent wall jet is focused. The effects of stokes number were explored and a decrease of particle stokes number was observed in the streamwise direction. More details of existing pneumatic conveying systems research and related numerical approach can be found in many literatures (Patel *et al.* 1993; Dolatabadi *et al.* 2004; Rinoshika and Suzuki 2010; Bareschino *et al.* 2014; Setia *et al.* 2014; Liang *et al.* 2015; Setia *et al.* 2015b; Almohammed and Breuer 2016b; Dong Li *et al.* 2016; S. M. El-Behery *et al.* 2017).

Aiming to reveal more details of cement flow characteristics in a small-scale prototype ASC system and to demonstrate the robustness of the numerical techniques adopted here in modeling two-phase flows, the present study conducted both steady-state and transient simulations to verify the system design. In particular, it should be highlighted that the prototype design is based on the actual air-slide conveyor presently operated by Jurong Port Pte Ltd (i.e. the operator), Singapore. Hence, the simulation results provide information to better understand how the prototype (and hence the full-scale) ASC system can be improved to enhance cement-conveying capacity.

2. DESIGN DETAILS OF THE PROTOTYPE ASC

The design of the prototype ASC is shown in Fig. 1.

It was proposed as a simpler and cost-efficient model for laboratory test, as replacement of the actual industrial ASC. This prototype ASC was designed to be powered by air blowers along the bottom plenum/air chamber, and a cement chamber was designed and used for cement flow conveying purpose. A suction fan was located near the conveyor exit to aid cement delivery down the chamber. The cross-sectional dimensions ($w \times h$) of the cement channel are $0.315 \text{ m} \times 0.260 \text{ m}$ and those for the air channel are $0.315 \text{ m} \times 0.07 \text{ m}$. Note that the dimensions of the cement chamber are half those of the industrial ASC and as such, the cross-section areas are a quarter of those associated with the industrial ASC. The inclination of the system was $\alpha = 7^\circ$ as measured from the horizontal. The system worked by injection of air into the plenum/air chamber, where the pressurized air was further forced to travel through the porous membrane (i.e. stretched fabric). Upwards moving air exiting the fabric surface fluidized the cement layer within the cement chamber and induced the cement particles to flow down the chamber by gravity. Table 1 gives the comparison of the working dimensions and parameters between the prototype and industrial ASC. For the proposed ASC model, a significantly reduced total length of 4.3 m was used, due to limitations in the laboratory working space.

To assess the influence of particle flow dynamics upon the air flow, the dimensionless Stokes number St (defined as $St = (\rho_p d_p^2 U_0) / (18 \mu L_0)$) was used to characterize particle behaviour. According to the physical geometry and the specified operation condition of the system, the St number was predicted to be well within the order of 10^{-2} , indicating that cement particles follow the carrier fluid closely, as the St value is much less than one explained by Tropea *et al.* (2007). Therefore, the mixture velocity is representative of the air and cement velocity and will be used in discussions thereafter.

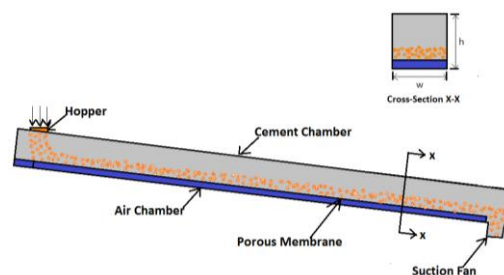


Fig. 1. Schematic diagram of the prototype ASC working process.

3. NUMERICAL APPROACHES AND PROCEDURES

Experimental limitations including cement dust storage limit, environmental issues and health concerns for researchers, have led to difficulties in the experiments with the prototype ASC system in a laboratory environment. As such,

state-of-the-art numerical techniques offer an alternative and reliable approach to investigate the problem. Both steady-state and transient simulations were conducted to aid the analysis of the prototype ASC, the procedures of which will now be presented in greater detail. It should be noted that, in contrast to an earlier study by Xiang *et al.* (2017) where the focus was on the industrial ASC system, the present study focuses on how capable numerical simulations are in modelling flow details of the prototype ASC system and how they match up with earlier simulations on the industrial ASC.

Table 1 Comparison of ASC between operator’s design and the prototype

Air-slide conveyor	Operator’s design	Prototype design
Length	94 m	4.3 m
Cement chamber width	0.63 m	0.315 m
Cement chamber height	0.52 m	0.26 m
Cross-sectional area	0.328 m ²	0.082 m ²
Air chamber height	0.07 m	0.07 m
Pressure	0.06 bar	0.06 bar
Air-superficial velocity	3 m/s	3 m/s
Inclination	7°	7°
Aspect ratio (AR=bed depth/bed width)	100/630=0.16	50.4/315=0.16

A three-dimensional computational domain was generated using Gambit-2.4 based on the physical dimensions of the prototype ASC. The domain includes several sub-domains for air/cement chambers to aid mesh generation, in contrast to the single air/cement chamber in practice. Nevertheless, continuous air/cement chambers are maintained. Five identical square air-inlet faces are specified on the plenum/air chamber bottom wall to introduce air into the system. The hopper was modeled as installed above the cement chamber and the suction fan was modeled as installed below the cement chamber near system exit.

Structure computational mesh was built throughout the flow domain with Gambit-2.4. Organized and structured mesh were built for each sub-domain, which were linked to form continuous flow path for air chamber and cement chamber respectively. In total, 2.58 million mesh cells were constructed after a mesh independence study. The maximum skewness of mesh cells is 0.56 and over 98.8% of cells are with skewness less than 0.1, indicating a high quality mesh had been achieved. Good mesh quality is of paramount importance as it ensures the convergence of simulation and the accuracy of simulation results, especially for complex

particle-laden flow problems like the one investigated here.

The simulation operating conditions were specified based on the material properties and experiment facility capabilities, with similar simulation procedures applied based on the earlier work by Xiang *et al.* (2017). Table 2 gives the simulation input parameters. Ordinary cement Portland with a constant mean particle size of 14 μm was defined in the simulations by Mills (2003), where no particle size variations (Bentz *et al.* 1999a; Bentz and Haecker 1999b) and no particle coagulation due to humidity was considered within the scope of the present study. The bulk density was defined as $\rho_{bulk} = 1362 \text{ kg/m}^3$ due to packing limit and the fluidized density was calculated based on the volume fraction of cement from the hopper. Two different volume fractions of cement, i.e., 0.3 and 0.1 respectively, are applied in the present calculation, resulting in two different fluidized density values as given in Table 2. Accordingly, specific solid load ratio (SLR) comparable with those used by the operator is maintained. The conveyor incline angle used was $\alpha = 7^\circ$, similar to the industrial ASC. A constant volume flow rate of 2 m³/min based on air-fan design capacity was specified for each predefined air injection location at the plenum chamber bottom wall. The mixture velocity at hopper was defined as 4 m/s according to industrial system reference value and would be the free air superficial velocity. A suction fan was modeled near cement chamber exit with a specified constant value of $P_{suction} = -2500 \text{ pa}$, which is the measured data from operator’s working condition. Lastly, simulations were performed with ANSYS Fluent 15.0 software, where the mixture model, i.e, a simplified Eulerian approach, is used to treat the dispersed-phase and the continuous phase as interpenetrating continua to ensure cost-efficiency and computation accuracy. Simulations are performed with High Performing Computing Cluster, where parallel computing was utilized.

Table 2 Input Parameters for Simulations of the prototype ASC

Material type	Cement portland
Mean particle size	14 μm
Bulk density	1362 kg/m ³
Conveyor inclination	7°
Air fan blower flow rate	2 m ³ /min
Mixture velocity at hopper	4 m/s
Suction fan pressure	-2500 Pa
Test 1 Cement volume fraction	0.3
Test 2 Cement volume fraction	0.1
Test 1 Fluidized density & SLR	408.6 kg/m ³ , SLR = 476.5
Test 2 Fluidized density & SLR	136.2 kg/m ³ , SLR = 123.5

4. RESULTS AND DISCUSSIONS

4.1 Steady-State Simulations

Firstly, steady-state simulation results will be presented and discussed here, where each simulation was performed using 16 processors with 12 hours computing time and 10,000 iterations were required to achieve a converged solution. In particular, simulation results for SLR = 476.5 test case (i.e. similar SLR for the industrial ASC) were analyzed and will be discussed here unless otherwise specified. Fig. 2(a) shows the cement distribution adjacent to the prototype ASC side-wall. Cement granule clouds are captured, which lead to accumulation of cement adjacent to conveyor side wall. The cement accumulation can be attributed to the spinning motion of flow near wall-fabric corners, causing cement particles to lose momentum in those regions. Besides that, Fig. 2(b) presents the cement distributions along the prototype ASC mid-span section. Different from the near-wall distribution seen earlier, cement particles tend to settle down near the fabric surface and thus demonstrating non-uniform air injection distributions through the fabric surface from the plenum/air chamber. Critical flow features such as a highly turbulent flow and accumulation of cement particles in certain regions have also been captured by the simulations.

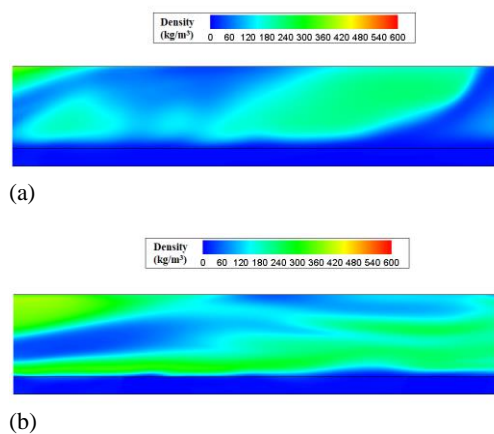


Fig. 2. Cement distributions (a) adjacent to ASC side wall and (b) at ASC mid-span section.

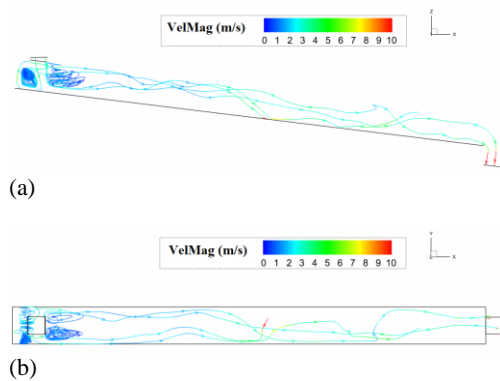


Fig. 3. Streamlines initiated from the hopper - (a) side-view and (b) top-view.

Figure 3 shows the mixture streamlines associated with the two-phase flow discharging from the hopper, where both side- and top-views are presented to better showcase the flow developments. Recirculating flow regions upstream of the hopper can be identified near the hopper in Fig. 3(a), where clock-wise rotations of cement flows are observed. Air exiting upwards from the fabric surface and cement flow discharging downwards from the hopper interact to give rise to these recirculating regions. Interestingly, a pair of vortices is formed downstream of hopper as well, as shown in Fig. 3(b), and they are postulated to be due to the flow blockage caused by the discharging cement right at the hopper location. On one hand, the existence of these recirculating flow systems in the hopper region prevents cement particles from settling down immediately on the fabric surface, this allowing them to flow downstream. On the other hand, it also meant that the cement flow can be further optimized if the recirculating flow regions upstream of the hopper can be mitigated. Nevertheless, these recirculating flow regions are limited to close vicinity of the hopper, and the cement flow resumes its journey along the fabric further downstream.

Figure 4 shows the pressure distribution in the prototype ASC, where pressure value decreases continuously from beyond the vicinity of the hopper to the exit. Low pressure regions are also noted to exist immediately upstream and downstream of the hopper location, which is linked to the recirculating regions discussed earlier. Such a pressure distribution along that region indicate that this phenomenon may be self-reinforcing, as an adverse pressure gradient exists downstream where it may encourage the recirculating regions to persist. Further downstream, favorable pressure gradient provides the impetus for the cement to propagate down the cement chamber, assisted by the modeled gravity force and suction fan. As for the air chamber, high pressure is observed throughout due to the pressurized air injected into it and crossing the fabric under a higher working pressure.

Figure 5 shows the VelMag distribution in the prototype ASC system. Higher velocity flows mainly exist in the downstream region of the cement chamber, due to the favorable pressure gradient mentioned previously. Very high velocity flow regions also exist at the air injection and suction fan locations, due to air forcing and suction functions respectively. Lower velocity flow regions are observed to be located upstream and downstream of the hopper location, prevailing for about the first 40% length of the cement chamber. Flow recirculation zones with low velocities coincide with high-pressure regions in the cement chamber seen in Fig. 4 earlier as well. It is also interesting to note that the velocities associated with the pressurized air decreases rapidly after impinging upon the fabric within the air chamber.

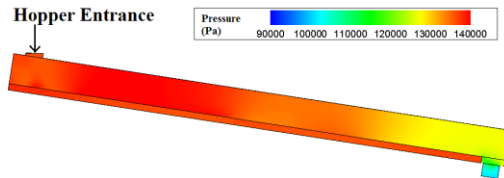


Fig. 4. Global pressure distributions in the prototype ASC system.

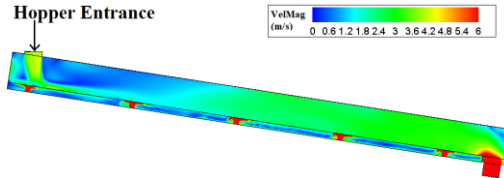


Fig. 5. Global VelMag distributions in the prototype ASC system.

Figure 6 shows comparisons of cement distributions along xz planes at different y locations. Here, $y = 0$ m represents mid-span plane while $y = 0.15$ m represents plane adjacent to the side-wall. Similar to what were observed earlier in Fig. 3, cement flow tends to develop better away from the side-walls, as wall effects are less significant and cement accumulation is reduced. Cement clouds are diluted by air and well-conveyed downstream in the main flow region. Fig. 7 shows another similar comparison, but at a lower operation load of $SLR = 123.5$. Similar to the benchmark test at $SLR = 476.5$, cement clouds are identified in upstream and side-wall regions. A more obvious circulation zone exists upstream of the hopper and cement flow is generally better fluidized, a significant difference from the benchmark test. Cement flow appears to be significantly more coherent and cement conveying is smoother throughout the cement chamber. Minor cement clouds are still produced near the side-wall, demonstrating they are formed regardless of the operation load levels. These results show that cement flow fluidizes better with a lower operation load, which provides smoother transportation of cement particles within the system. Despite that however, a higher operation load will be desirable since it leads to higher conveying capacity and efficiency.

Next, the suction fan pressure was adjusted to look into its effects on the overall cement mass flow rate (\dot{m}) in the present prototype ASC. It should be noted that the pressure values specified here represent predefined pressure drop at the system exit, where five different pressure values ranging from 0 to 20000 Pa are defined. Fig. 8 shows the achievable mass flow rates at different suction fan pressures. Pressure drop amplification results in an increment of output cement mass flow rate, where 45% enhancement of output mass flow rate can be achieved within the pressure drop investigated here. This trend confirms the conclusions reached in an earlier study for the actual ASC system by Xiang *et al.* (2017), which was validated by actual industrial operational data, that the presence of a suction fan enhances the conveying capability of air-slide

system significantly. Hence, it suggests that further enhancements in cement conveying can be achieved by adjusting the pressure drop at the conveyor exit.

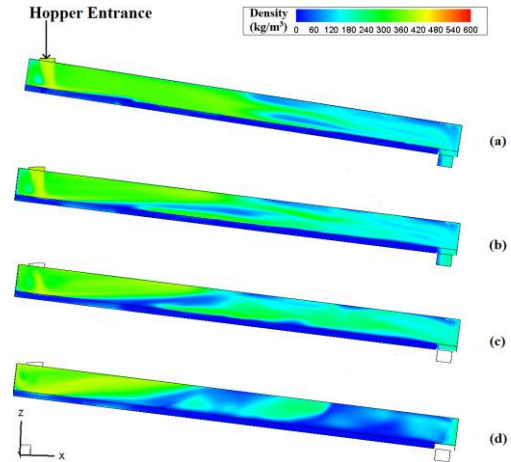


Fig. 6. Cement distributions along xz planes at different y locations, (a) $y = 0$ m, (b) $y = 0.05$ m, (c) $y = 0.1$ m and (d) $y = 0.15$ m. Simulations conducted with $SLR = 476.5$.

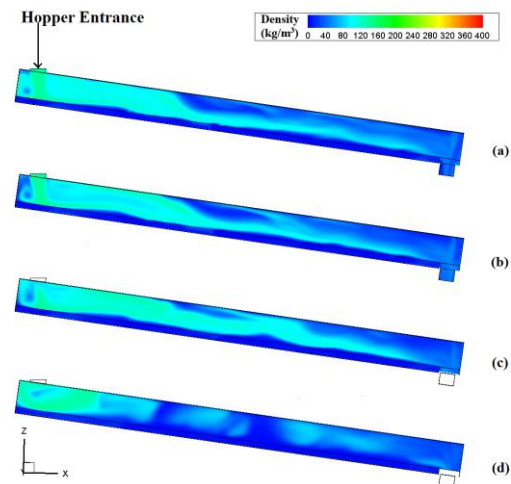


Fig. 7. Cement distributions along xz planes at different y locations, (a) $y = 0$ m, (b) $y = 0.05$ m, (c) $y = 0.1$ m and (d) $y = 0.15$ m. Simulations conducted with $SLR = 123.5$.

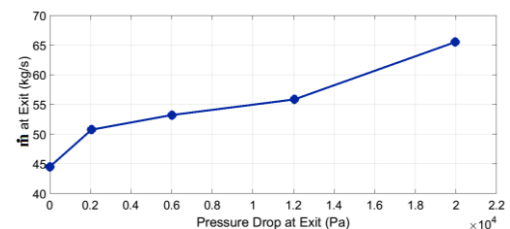


Fig. 8. Variations of cement mass flow rate with suction fan pressure.

4.2 Transient Simulation

A transient simulation was also performed to investigate the cement flow behavior temporally. A refined computational mesh was generated to

improve the resolution for the present transient simulation. In total, 6.39 million mesh cells were used, which was more than twice that of the mesh used for steady-state simulation (2.58 million). Note that the benchmark test condition of SLR = 476.5 remain the focus of the present transient simulation. A time-step of $\Delta t = 0.001$ s was used for a total run time of $t=10$ s, which was sufficient long for the flow to develop with time at a reasonable computational cost. The simulation took 10,000 iterations with a total of 144 hours computation time, with 32 processors on NTU-HPC cluster. Additionally, simulation data was saved at every 100 time-steps ($\Delta t = 0.1$ s), to aid data analysis during post-processing.

Following the procedures adopted for the earlier steady-state simulations, cement mass flow rate (\dot{m}) was monitored from $t = 0$ s to 10 s, so as to look the mass conservation during operation. Fig. 9 presents the history of the exit mass flow rate, as indicated by the red line. The mass flow rate histories monitored at the hopper entrance and air-inlet are plotted as references, which show fairly constant values during the simulation. Between $t = 0$ s to 5 s, the absolute value of the exit mass flow rate increases, due to the starting process. After $t = 5$ s, the mass flow rate history shows significant fluctuations, with the mass flow rate surging and reducing as a result of stochastic settlement and movement of cement particles in the cement chamber. Between $t = 5$ s to 10 s, the mass flow rate captured at the hopper entrance is approximately $\dot{m} = 37.2$ kg/s, while the time-averaged mass flow rate at the exit is estimated to be $\dot{m} = 36.6$ kg/s. As such, the mass flow rate histories demonstrate satisfactory mass balance within the system, with only about 1.7% difference in their values. The slight loss of exit mass flow rate can be explained by cement settlement on fabric surface and ASC corner regions, and hence does not undermine the mass balance conclusion drawn here. The transient simulation results suggest that formation of cement clouds or occasional cement settlement will not affect total conveying capability of the system with the present operation condition significantly. Besides that, transient simulation offers a feasible approach to predict cement surge and drop within the system on a temporal basis, which is of practical implications in terms of actual operations. Nevertheless, it should still be noted that the simulation was conducted at ideal conditions, where effects of humidity and cement particle size variations were not considered. Other potential factors including wall roughness and non-constant hopper loading may affect cement distribution to some extent as well.

Figure 10 shows the history of absolute pressure monitored at the system exit between $t = 0$ s to 10 s, with an initially specified suction fan pressure drop of 20,000 Pa. From $t = 0$ s to 2 s, severe fluctuations in the pressure variation can be observed, due to the starting process. After $t = 2$ s, the pressure value stabilizes with only minor

variations, when cement flow begins to develop better. Simulation results show that the exact pressure drop at system exit impacts significantly upon the initial flow characteristics, after which the transient nature of cement flow contributes more towards flow fluctuations and mass flow rate variations.

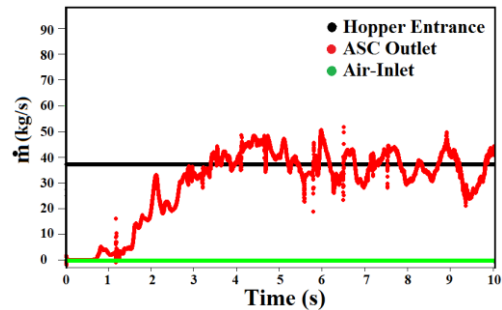


Fig. 9. Time histories of mass flow rates between $t = 0$ s to 10 s.

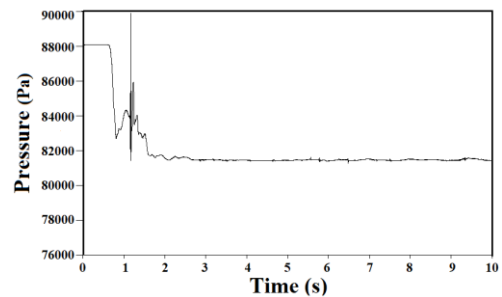


Fig. 10. Time history of absolute pressure at the system exit between $t = 0$ s to 10 s.

The distribution of mixture velocity on time-basis in the system is presented in Fig. 11. Five different locations ((a), (b), (c), (d) and (e)) are selected in the cement chamber and data lines are drawn on the Mid-span section as shown in Fig. 11(f) as an illustration. Normalized (h/H) values represent distance from cement chamber ceiling, where $H = 0.26$ m is the height of cement chamber. Transient simulation data from $t = 6$ s to $t = 10$ s is used, representing the fully developed flow. In Figs 11((a), (b)), velocity distribution deviate significantly at different flow time. This phenomenon can be attributed to the influence of flow from hopper. Interestingly, no significant deviation of velocity is identified near fabric region in Fig. 11(a) due to the suppression hopper flow on the air injection, while large deviations are observed near fabric region for Figs 11 ((b), (c), (d), (e)) where hopper flow effect is minor. Also, In Figs 11((c), (d), (e)) velocity distributions on time-basis are more uniform from $t = 7$ s onwards, showing that flow is better developed in the downstream.

The averaged mixture velocity distribution along the streamwise direction of the system is presented in Fig. 12. Ten cross-sectional planes in cement chamber along the system are selected and averaged velocity values for each flow time ($t = 6$ s to $t = 10$ s) are calculated. Normalized (l/L) represents

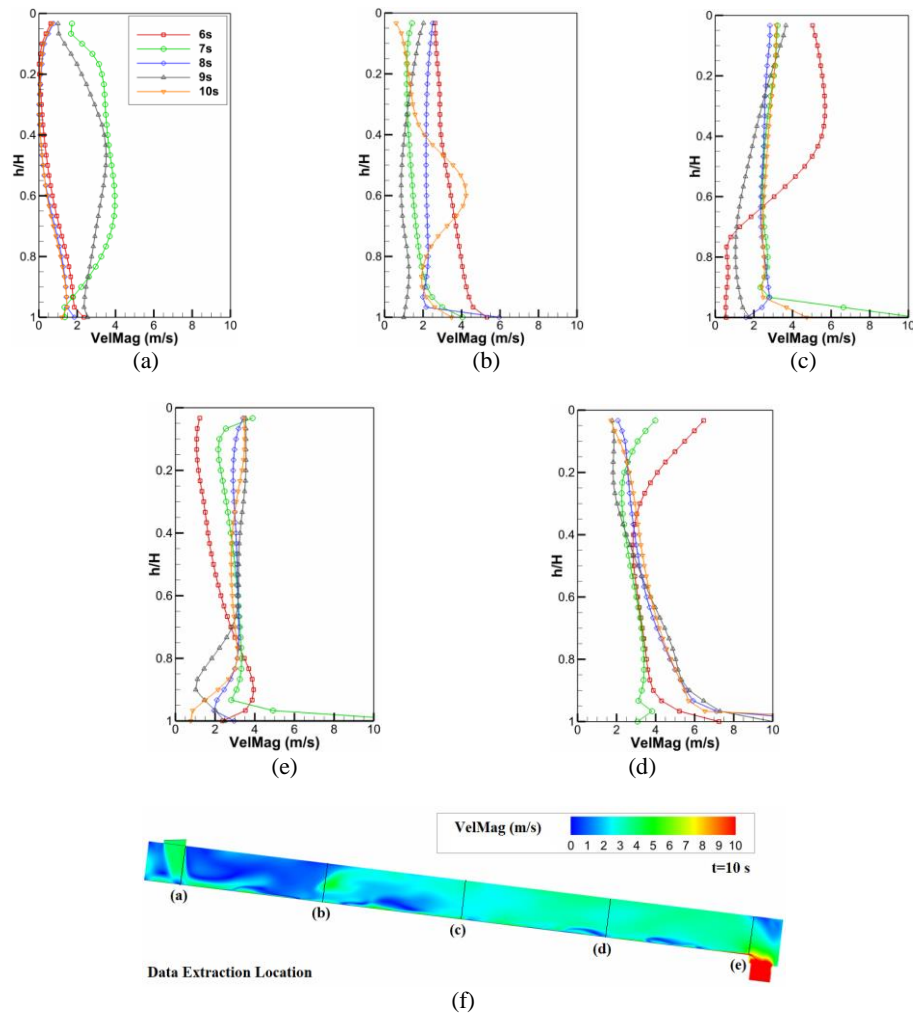


Fig. 11. Velocity distribution at different data extraction locations from $t=6$ s to $t=10$ s.

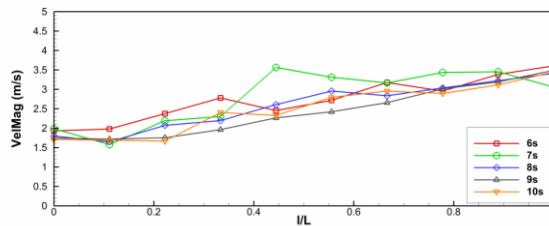


Fig. 12. Averaged velocity distribution on different cross-sectional planes along the system from $t=6$ s to $t=10$ s.

locations of cross-sectional planes, where $L = 3.7$ m is the total length of the main flow region, i.e., hopper entrance and suction fan regions are not included. Though general consistency of velocity is observed with a steady increase of velocity values at all flow time, some deviations are still identified for $t = 7$ s results in certain regions. At $t = 7$ s, higher velocity is observed from $l/L = 0.44$ onwards, which could be an interactive result of disturbance of hopper flow and air injection from fabric surface. Yet, this higher value of velocity region is only observed at $t = 7$ s, suggesting an instant agitated flow pattern within the system. Whether cyclic flow patterns will be observed

during longer operation is yet to know from the present simulation work, due to the limitation of computational resources allocated. Further investigations should be proposed to clarify this issue.

5. CONCLUSIONS

This study presents numerical investigation on a prototype ASC, based on industrial design. Both steady-state and transient simulations are performed, to identify critical flow features within the prototype ASC and to demonstrate the validity of the prototype ASC design.

Simulation results reveal details of cement flow characteristics within the system. The cement flow is identified highly disturbed within the system, with cement clouds or settlement in conveyor corner and side wall regions identified. The cement settlement in those regions is minor compared with the total mass flow rate, where mass balance within the system is demonstrated with less than 2% loss of mass monitored from system exit. Besides that, lower operation load (SLR) leads to more coherent cement flow, though it also raises concern of compromise in the conveying capacity of the system. The design of suction fan contributes to enhanced conveying capability of the system, by enhancing cement fluidity especially near system downstream region. Transient simulation results present more details of cement flow patterns on temporal basis. Fluctuation of mass flow rate monitored at system exit is observed, though the fluctuation pattern is proved to have only minor effect on the total mass flow rate within the system. The pressure fluctuates severely during the starting process of the system, which contributes to the agitated flow patterns for the first 2 s, after that, the transient nature of flow dominates the flow fluctuation and mass flow variations. Deviations of velocity distribution on temporal basis are also observed for certain flow time, proving the instantaneous agitated flow and transient nature of flow within the present system.

This study paves the way for using similar numerical tools to investigate air-slide conveyor system, with critical flow features captured in both steady-state and transient simulations. Apart from that, simulation results build confidence that cement is well transported by the air phase so long as the system operates within its capacity. The prototype design is proved comparable with the actual ASC and feasible for cement transportation operation. Optimization of the actual ASC system can be proposed on the foundation of this simulation work, to enhance cement transportation.

REFERENCES

- Almohammed, N. and M. Breuer (2016a). Modeling and simulation of agglomeration in turbulent particle-laden flows: A comparison between energy-based and momentum-based agglomeration models. *Powder Technology* 294, 373-402.
- Almohammed, N. and M. Breuer (2016b). Modeling and simulation of particle-wall adhesion of aerosol particles in particle-laden turbulent flows. *International Journal of Multiphase Flow* 85: 142-156.
- Bareschino, P., R. Solimene, R. Chirone and P. Salatino (2014). Gas and solid flow patterns in the loop-seal of a circulating fluidized bed. *Powder Technology* 264, 197-202.
- Bentz, D. P. and C. J. Haecker (1999a). An argument for using coarse cements in high-performance concretes. *Cement and Concrete Research* 29(4), 615-618.
- Bentz, D. P., E. J. Garboczi, C. J. Haecker and O. M. Jensen (1999b). Effects of cement particle size distribution on performance properties of Portland cement-based materials. *Cement and Concrete Research* 29(10), 1663-1671.
- Cong, X., X. Guo, X. Gong, H. Lu and W. Dong (2011). Experimental research of flow patterns and pressure signals in horizontal dense phase pneumatic conveying of pulverized coal. *Powder Technology* 208(3), 600-609.
- Dolatabadi, A., J. Mostaghimi and V. Pershin (2004). Modeling Dense Suspension of Solid Particles in Highly Compressible Flows. *International Journal of Computational Fluid Dynamics* 18(2), 125-131.
- Gupta, S. K., V. K. Agarwal, S. N. Singh, V. Seshadri, D. Mills, J. Singh and C. Prakash (2009). Prediction of minimum fluidization velocity for fine tailings materials. *Powder Technology* 196(3), 263-271.
- Gupta, S. K., V. K. Agrawal, S. N. Singh, V. Seshadri and D. Mills (2006). An experimental investigation on a fluidized motion conveying system. *Powder Technology* 167(2), 72-84.
- Li, D., A. Wei, K. Luo and J. Fan (2016). Direct numerical simulation of a particle-laden flow in a flat plate boundary layer. *International Journal of Multiphase Flow* 79, 124-143.
- Li, K., S. B. Kuang, R. H. Pan and A. B. Yu (2014). Numerical study of horizontal pneumatic conveying: Effect of material properties. *Powder Technology* 251, 15-24.
- Liang, C., J. R. Grace, L. Shen, G. Yuan, X. Chen and C. Zhao (2015). Experimental investigation of pressure letdown flow characteristics in dense-phase pneumatic conveying at high pressure. *Powder Technology* 277, 171-180.
- Lungu, M., J. Wang and Y. Yang (2015). Numerical simulations of flow structure and heat transfer in a central jet bubbling fluidized bed. *Powder Technology* 269, 139-152.
- Mills, D. (2003). Pneumatic conveying design guide, Elsevier.
- Mittal, A., S. S. Mallick and P. W. Wypych (2015). An investigation into pressure fluctuations for fluidized dense-phase pneumatic transport of fine powders. *Powder Technology* 277, 163-170.
- New, T. H. and E. Tsioli (2011). An experimental study on the vortical structures and behaviour of jets issuing from inclined coaxial nozzles. *Experiments in Fluids* 51(4), 917-932.
- New, T. H. and J. Long (2015). Dynamics of laminar circular jet impingement upon convex cylinders. *Physics of Fluids* 27(2), 024109.
- Patel, M. K., K. Pericleous and M. Cross (1993). Numerical modelling of circulating fluidized beds. *International Journal of Computational*

- Fluid Dynamics* 1(2), 161-176.
- Pu, W., C. Zhao, Y. Xiong, C. Liang, X. Chen, P. Lu and C. Fan (2010). Numerical simulation on dense phase pneumatic conveying of pulverized coal in horizontal pipe at high pressure. *Chemical Engineering Science* 65(8), 2500-2512.
- Rinoshika, A. and M. Suzuki (2010). An experimental study of energy-saving pneumatic conveying system in a horizontal pipeline with dune model. *Powder Technology* 198(1), 49-55.
- S. M. El-Behery, A. A. El-Haroun and M. R. Abuhegazy (2017). Prediction of pressure drop in vertical pneumatic conveyors. *Journal of Applied Fluid Mechanics* 10(2), 519-527.
- Setia, G. and S. S. Mallick (2015a). Modelling fluidized dense-phase pneumatic conveying of fly ash. *Powder Technology* 270 (A), 39-45.
- Setia, G., S. S. Mallick and P. W. Wypych (2014). On improving solid friction factor modeling for fluidized dense-phase pneumatic conveying systems. *Powder Technology* 257, 88-103.
- Setia, G., S. S. Mallick, R. Pan and P. W. Wypych (2015b). Modeling minimum transport boundary for fluidized dense-phase pneumatic conveying systems. *Powder Technology* 277, 244-251.
- Tropea, C., A. Yarin and J. F. Foss (2007). *Springer Handbook of Experimental Fluid Mechanics*, First edition, Springer. ISBN 978-3-540-30299-5.
- Wang, L.-P., C. Peng, Z. Guo and Z. Yu (2016). Lattice Boltzmann simulation of particle-laden turbulent channel flow. *Computers & Fluids* 124, 226-236.
- Wang, X., X. Zheng and P. Wang (2017). Direct numerical simulation of particle-laden plane turbulent wall jet and the influence of Stokes number. *International Journal of Multiphase Flow* 92, 82-92.
- Xiang, J., J. Heng and T. H. New (2017). A numerical parametric and optimization study of an industrial air-slide conveyor system. *Powder Technology* 315, 367-378.
- Yan, F. and A. Rinoshika (2013). High-speed PIV measurement of particle velocity near the minimum air velocity in a horizontal self-excited pneumatic conveying of using soft fins. *Experimental Thermal and Fluid Science* 44, 534-543.